Inorganic Chemistry

pubs.acs.org/IC Article

Probing the Axial Distortion Effect on the Magnetic Anisotropy of Octahedral Co(II) Complexes

Yi-Fei Deng, Mukesh Kumar Singh, Dexuan Gan, Tongtong Xiao, Yinuo Wang, Shihao Liu, Zhenxing Wang, Zhongwen Ouyang, Yuan-Zhu Zhang,* and Kim R. Dunbar*

Cite This: *Inorg. Chem.* 2020, 59, 7622–7630 Read Online

ACCESS | Metrics & More | Article Recommendations | Supporting Information

ABSTRACT: Three mononuclear octahedral Co(II) complexes are reported, $[Co(py)_4(SCN)_2]$ (**1**), $[Co(py)_4(Cl)_2]\cdot H_2O$ (**2**), and $[Co(py)_4(Br)_2]$ (**3**), that exhibit different distortions with compression (**1**) or elongation (**2** and **3**) of the axial positions. Easy plane magnetic anisotropy was confirmed by magnetic, HF-EPR, and computational studies for all complexes. Further analyses indicate that both the sign and magnitude of zero-field splitting parameters experience a significant change ($D \geq \pm 150$ cm^{-1}) by tuning of the axial and equatorial ligand field strength. Slow magnetic relaxation is observed for all compounds which is dominated by the Raman process involving both acoustic and optical phonons.

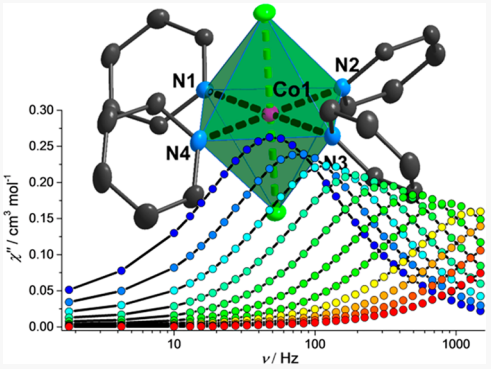

INTRODUCTION

Single-molecule magnets (SMMs)[1] are being investigated by chemists and physicists owing to their potential applications associated with data storage,[2] quantum computing,[3] and molecular spintronics.[4] In the pursuit of high-performance SMMs, a critical issue is to understand magnetostructural correlations. In this vein, the simplest models are mononuclear SMMs with significant anisotropy, often referred to as single-ion magnets (SIMs),[5] which are ideal prototypes for gaining insight into paramagnetic relaxation phenomena compared to more complicated large spin ground-state polynuclear compounds.[6,7]

A key underpinning of research on the topic of mononuclear SMMs is the opportunity to maximize uniaxial magnetic anisotropy arising from the crystal field for both the f- and d-block elements with the spin−orbit coupling (SOC) being much stronger for the rare earth elements.[8] Crystal-field theory underscores the importance of the local coordination environment and ligand-field strength on the electronic structures of metal ions, as found for a number of lanthanide SMMs in recent years.[9] As for 3d analogues, first order orbital angular momentum is typically quenched or diminished due to the low symmetry ligand-field environment with the magnetic anisotropy often arising from mixing of the electronic ground and excited states which is of the second order type.[5d−f] Clearly strict regulation of ligand geometry is important for preserving first-order SOC in order to achieve high magnetic anisotropy for mononuclear 3d SMMs.

The exquisite sensitivity of magnetic anisotropy to changes in coordination environment is one of the main challenges for synthetic chemists in the design of high performance SMMs.[10] Representatives of 3d SMMs with a high degree of magnetic anisotropy arising from first SOC are found in low-coordinate metal complexes, which exhibit high effective energy barriers comparable to the lanthanide SMMs under zero dc fields.[11] This situation notwithstanding, theoretical predictions support the contention that higher-coordinate mononuclear 3d metal complexes are also capable of exhibiting appreciable magnetic anisotropy from enhanced second order SOC;[12] these examples include six-coordinate Co(II) complexes.[13] Both easy-axis and easy-plane types of magnetic anisotropy have been reported for Co(II) complexes with distorted octahedron geometries although most of them fall into the latter category. These literature reports reveal that the sign of the zero-field splitting (zfs) parameter is related to the coordination geometry of Co(II) ions, the ligand field, and even the secondary coordination environment. Given the complexity of these combined factors, specific effects on magnetic anisotropy are often difficult to extract. Clearly, systematic studies of magnetostructural correlations are essential for a better understanding of the magnetic anisotropy and relaxation dynamics in Co(II) systems.

Received: February 19, 2020
Published: May 11, 2020

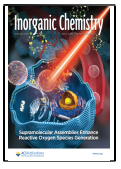

https://dx.doi.org/10.1021/acs.inorgchem.0c00531
Inorg. Chem. 2020, 59, 7622–7630

Table 1. X-ray Crystallographic Data for 1−3

	1	2	3
Empirical formula	$C_{22}H_{20}CoN_6S_2$	$C_{20}H_{22}Cl_2CoN_4O$	$C_{20}H_{20}Br_2CoN_4$
Formula weight/g mol^{-1}	491.49	464.24	535.15
crystal system	Monoclinic	Monoclinic	Orthorhombic
space group	$C2/c$	$P2_1/n$	$Pna2_1$
a, Å	12.289(6)	9.263(4)	15.850(4)
b, Å	12.991(7)	16.597(7)	9.393(2)
c, Å	14.869(8)	13.794(6)	14.052(3)
α, deg	90	90	90
β, deg	107.536(6)	94.715(5)	90
γ, deg	90	90	90
V, Å^3	2263(2)	2113.6(15)	2092.2(8)
Z	4	4	4
d_{cal}/g cm^{-3}	1.442	1.459	1.699
Temperature, K	110(2)	110(2)	110(2)
Radiation	MoKα	MoKα	MoKα
θ range	2.34−27.67°	3.54−25.02°	2.52−27.49°
completeness	99.2%	99.1%	100%
residual map, e Å^{-3}	0.278/−0.284	0.304/−0.292	0.321/−0.413
Goodness-of-fit on F^2	1.057	1.021	1.017
R indices [$I > 2\sigma(I)$]	R_1 = 0.0295, wR_2 = 0.0677	R_1 = 0.0314, wR_2 = 0.0703	R_1 = 0.0263, wR_2 = 0.0493
R indices (all data)	R_1 = 0.0361, wR_2 = 0.0705	R_1 = 0.0455, wR_2 = 0.0776	R_1 = 0.0319, wR_2 = 0.0508

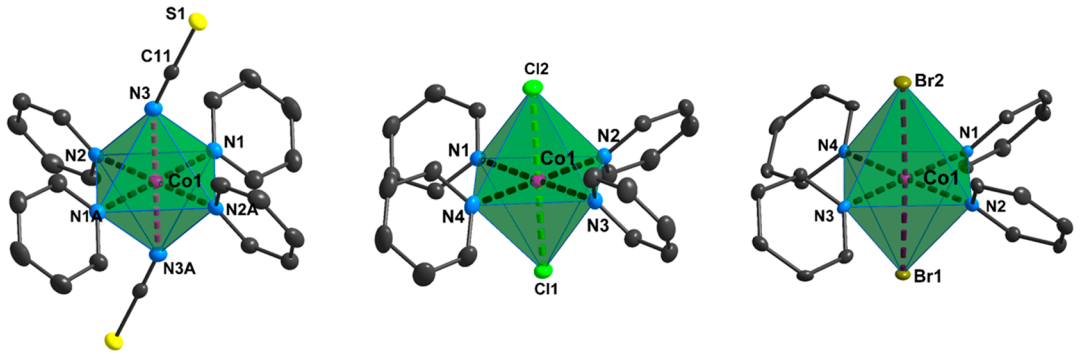

Figure 1. Molecular structures of complexes **1**−**3**. Thermal ellipsoids are drawn at the 50% level; all hydrogen atoms and interstitial solvent molecules are omitted for the sake of clarity.

Herein we report a magnetic study of three distorted octahedral Co(II) complexes, *viz.*, $[Co(py)_4(SCN)_2]$ (**1**), $[Co(py)_4(Cl)_2]\cdot H_2O$ (**2**), and $[Co(py)_4(Br)_2]$ (**3**), which all have pyridine ligands in the equatorial positions and thiocyanate, chloride, or bromide groups in the axial sites, leading to a compressed or elongated distortion along the axial direction. The differences caused by the axial ligand field contribute to a change in magnitude rather than the sign of D, as confirmed by combined magnetic and HF-EPR data. Field induced slow magnetic relaxation originating from a Raman process involving both acoustic and optical phonons[9h] is observed for all three derivatives. In addition, *ab initio* CASSCF/NEVPT2 calculations were performed to estimate the magnetic anisotropy parameters as well as to extract predictive correlations by altering both the axial and equatorial ligand fields which led to significant changes in both the magnitude and the sign of D.

RESULTS AND DISCUSSION

Synthesis and Crystallographic Studies. Compounds **1**−**3** (Table 1) were obtained by slow evaporation of a methanol solution containing the metal salts and pyridine (see Experimental Section in the Supporting Information). The molecules exhibit highly distorted six-coordinate octahedral environments with the two thiocyanate N atoms (for **1**) or two halogen atoms (Cl for **2**; Br for **3**) occupying the axial positions and the four pyridine N atoms defining the equatorial plane (Figure 1, Table S1). For **1**, the axial Co−$N_{thiocyanate}$ bond lengths (2.087(1) Å) are much shorter than the equatorial Co−N_{py} bond distances (2.191(1) Å, 2.201(1) Å), a clear indication of a compressed octahedral geometry. Different distortions are observed for **2** and **3**, for which the coordination spheres exhibit an elongation along the X−Co−X axis (Co(1)−Cl(1), 2.428(1) Å; Co(1)−Cl(2), 2.444(1) Å; Co(1)−Br(1), 2.620(1) Å; Co(1)−Br(2), 2.605(1) Å)) compared to the equatorial Co−N bond length (2.169(2)−2.195(2) Å for **2**; 2.165(4)−2.174(4) Å for **3**). The adjacent Co···Co separations are 8.09, 7.99, and 8.45 Å for **1**−**3**, respectively (Figure S4).

Magnetometry and HF-EPR Studies. Temperature dependent susceptibility was measured under a 1000 Oe dc field over the 2−300 K temperature range (Figure 2). The χT

https://dx.doi.org/10.1021/acs.inorgchem.0c00531
Inorg. Chem. 2020, 59, 7622−7630

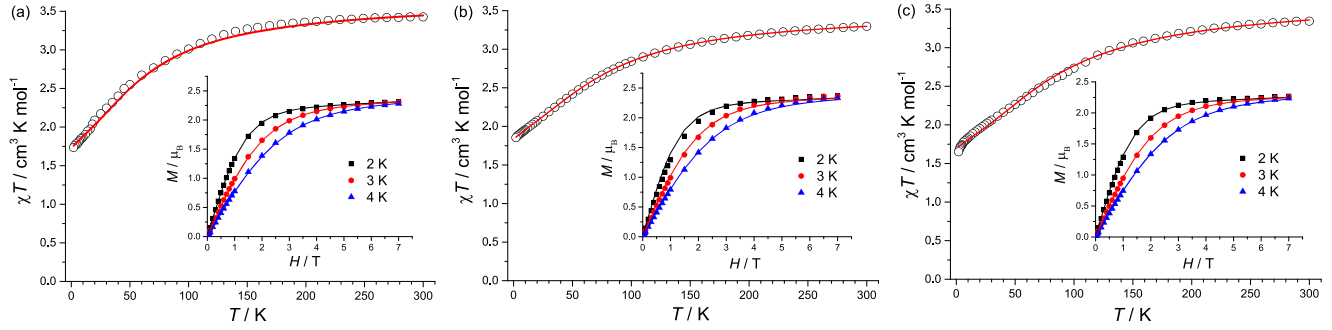

Figure 2. Temperature dependence of χT obtained at 1000 Oe (data points) for **1** (a), **2** (b), and **3** (c). Solid lines represent the fits with the PHI program. Inset shows the 2−4 K field-dependent magnetization and its fit obtained simultaneously with the χT fit.

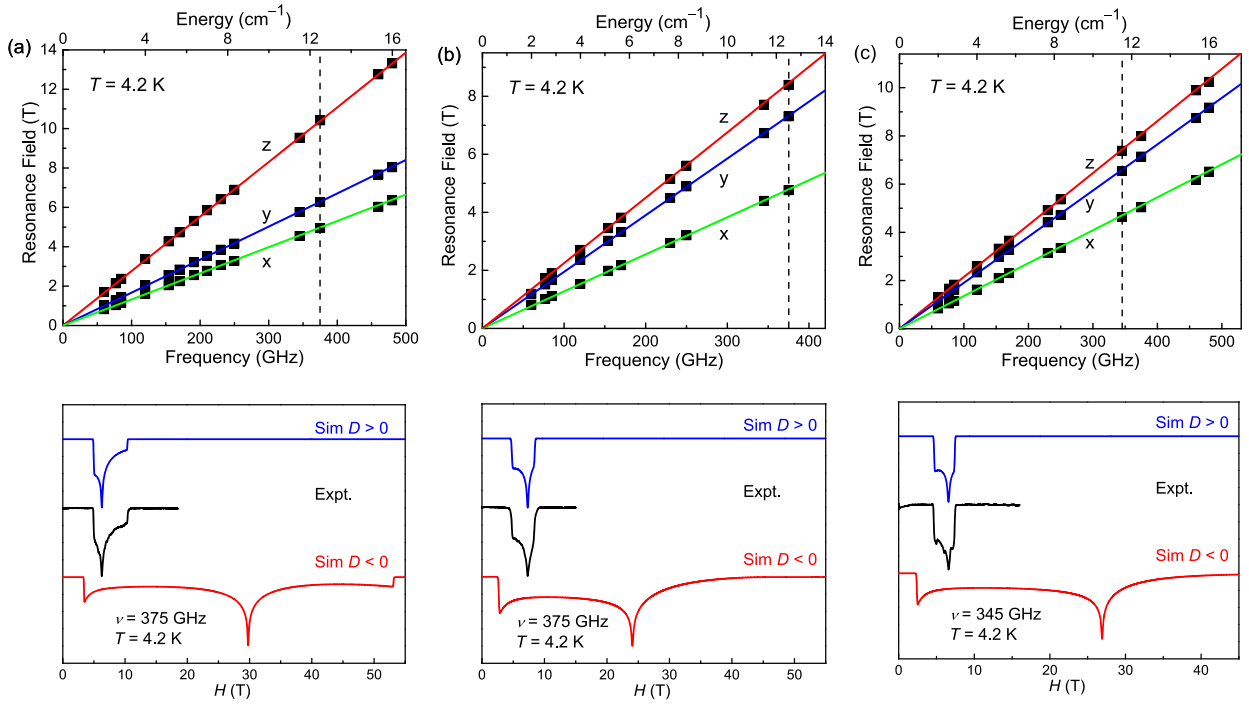

Figure 3. Resonance field vs microwave frequency (quantum energy) for EPR transitions and HF-EPR spectrum with its simulations at 4.2 K of **1** (a), **2** (b), and **3** (c). Green, blue, and red curves are the simulations using the best-fitted spin Hamiltonian parameters with the magnetic field H parallel to the x, y, and z axes of the ZFS tensor, respectively. The vertical dashed line represents the frequency used at which the spectra were recorded or simulated.

products of 3.43, 3.30, and 3.34 cm^3 K mol^{-1} for **1**−**3** at room temperature are in the normal range for an isolated high spin Co(II) ion with orbital contributions.[14] Upon cooling, χT decreases gradually above 100 K and drops more quickly at low temperature, indicating significant magnetic anisotropy of the Co(II) ions, as confirmed by the field-dependent magnetization data which do not saturate even at the highest fields. In order to gain insight into the magnetic anisotropy, χT *vs* T and M−H plots were fitted simultaneously with the PHI program[15] based on the following spin Hamiltonian (eq 1, with $g_x = g_y$):

$$\hat{H} = D(\hat{S}_z^{\,2} - S(S+1)/3) + E(\hat{S}_x^{\,2} - \hat{S}_y^{\,2}) + \mu_B \sum_{i=x,y,z} \hat{S}_i g_i B_i \quad (1)$$

where E is the rhombic ZFS parameter, μ_B is the Bohr magneton, g is the Landé factor, and B is the magnetic induction. The best fit was achieved with the following parameters: **1**: $g_x = g_y = 2.31(2)$, $g_z = 3.58(3)$, $D = +46.8(3)$ cm^{-1}, $|E| = 1.42(4)$ cm^{-1}; **2**: $g_x = g_y = 2.47(3)$, $g_z = 3.19(2)$, $D = +68.2(5)$ cm^{-1}, $|E| = 2.74(3)$ cm^{-1}; **3**: $g_x = g_y = 2.27(3)$, $g_z = 3.64(2)$, $D = +61.5(4)$ cm^{-1}, $|E| = 2.42(2)$ cm^{-1}. For all of the complexes, it was found that the sign of the D value is sensitive with no acceptable fits being obtained with a negative value. Also, the obtained spin Hamiltonian parameters are comparable to reported mononuclear Co(II) complexes with similar coordination geometries.[13]

To further determine the anisotropy parameters, tunable-frequency HF-EPR experiments were conducted at 4.2 K on polycrystalline samples of **1**−**3** (Figure 3, Figures S5−S7). HF-EPR spectra of **1**−**3** exhibit three signals which arise from the intra-Kramers transitions within the lowest doublet $M_S = \pm 1/2$ with $\Delta M_S = \pm 1$, typical for a spin 3/2 system with large and positive D values.[16] As the magnitude of D is beyond the frequency limit (480 GHz ∼ 16 cm^{-1}) of our instrument, no transitions between Kramers doublets $m_s = \pm 1/2$ and $m_s = \pm 3/$

https://dx.doi.org/10.1021/acs.inorgchem.0c00531
Inorg. Chem. 2020, 59, 7622−7630

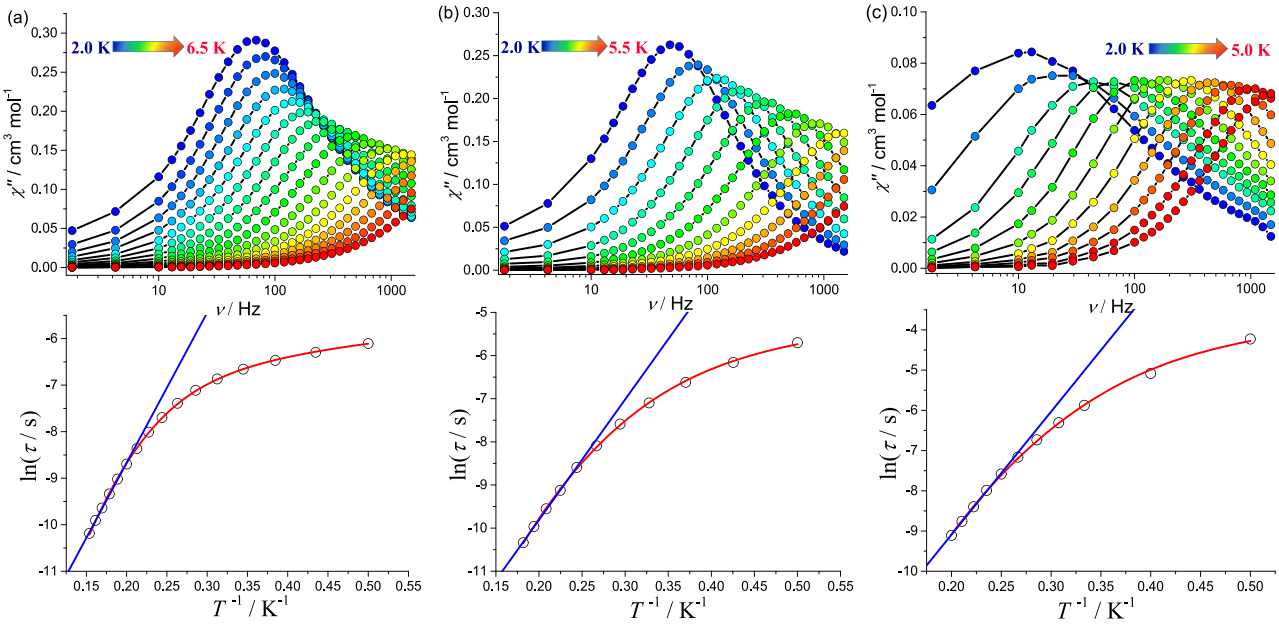

Figure 4. Frequency dependent magnetic susceptibilities of the out-of-phase signals and temperature dependence of the relaxation rates for **1** (a), **2** (b), and **3** (c) at indicated dc fields. The blue lines correspond to the high-temperature Arrhenius fitting, and the red lines represent the fitting based on eq 2.

Table 2. Parameters Obtained for the Fit of the Dependence of τ with Temperature at 1 kOe (for 1), 1.5 kOe (for 2), and 0.5 kOe (for 3) Using Linear Approximations and Eq 2

	1		2		3	
	linear approximation	fitted by eq 2	linear approximation	fitted by eq 2	linear approximation	fitted by eq 2
A, s^{-1} K^{-1}		218.5(5)		124.2(3)		27.3(8)
C, s^{-1} K^{-n}		0.15(2)		0.89(2)		0.16(3)
n		6.4(1)		6.2(1)		6.7(2)
τ_0, s	$2.7(3) \times 10^{-7}$		$2.1(2) \times 10^{-7}$		$3.3(2) \times 10^{-7}$	
U_{eff}, K	32.3(6)		27.9(4)		29.3(7)	

2 were observed, and the simulations were performed with the estimated D values from SQUID measurements. The best fit was obtained with the parameters: **1**: $g_x = g_y = 2.43(2)$, $g_z = 2.63(2)$, $D = +46.8(3)$ cm^{-1}, $|E| = 3.62(2)$ cm^{-1}; **2**: $g_x = g_y = 2.35(2)$, $g_z = 3.37(2)$, $D = +68.2(5)$ cm^{-1}, $|E| = 9.62(2)$ cm^{-1}; **3**: $g_x = g_y = 2.27(2)$, $g_z = 3.45(2)$, $D = +61.5(4)$ cm^{-1}, $|E| = 6.91(2)$ cm^{-1}.

Single-frequency spectra of **1** (375 GHz), **2** (375 GHz), and **3** (345 GHz) at 4.2 K were simulated as shown in Figure 3. A positive D value matches well the experiment whereas no reasonable simulations could be obtained when the sign of the D values was set to be negative. These results unambiguously corroborate the positive sign of the D value and the easy plane magnetic anisotropy of **1**−**3**.

Temperature and frequency dependences of the ac susceptibility measurements were conducted to probe the SMM behavior of **1**−**3** (Figure 4, Figures S8−S19). Under a zero dc field, no slow magnetic relaxation behavior was observed for the complexes, indicating considerable quantum tunneling of the magnetization (QTM).[17] Ac measurements under various dc fields were performed in order to determine the optimum field at which the QTM effects are minimized (Figures S8−S10); dc fields of 1 kOe, 1.5 kOe, and 0.5 kOe for **1**−**3**, respectively lead to frequency-dependent signals with obvious out-of-phase (χ'') peaks (Figures S11−S16). Such behavior is indicative of superparamagnetic-like slow magnetic relaxation of a SIM.

The least-squares fittings of the plots of χ'' versus χ' (known as Cole−Cole plots,[18] Figures S17−S19) based on the generalized Debye model[1a] produced relaxation times (τ) as well as the distribution coefficients α (Table S2). The relaxation times were plotted versus T^{-1}, generating Arrhenius plots and giving an estimation of the thermal energy barrier of 32.3(6), 27.9(4), and 29.3(7) K for **1**−**3**, respectively (Figure 4, Table 2).

Among the reported systems with easy plane magnetic anisotropy, the mechanisms responsible for the slow magnetic relaxation are generally summarized in two distinct ways.[19] One of them arises from a field-induced phonon effect,[19a−c] where the spin system follows an efficient Orbach relaxation pathway through the excited $M_S = +3/2$ levels. The other mechanism is ascribed to a transverse anisotropy barrier owing to a considerable E value.[19d] Neither mechanism appears to be applicable to the present compounds, however, due to the small effective energy barrier and experimental E values, which indicate that the magnetic relaxation most likely proceeds through a Raman process involving a virtual state.[19e]

It is notable that a Raman process has significant contributions to the behavior of reported Co(II)-based SIMs with the octahedron; nevertheless, a direct one-phonon contribution should not be neglected under a dc field at low

https://dx.doi.org/10.1021/acs.inorgchem.0c00531
Inorg. Chem. 2020, 59, 7622−7630

temperature. Therefore, we employed a model including direct and Raman relaxation mechanisms with the expression (eq 2)[20]

$$\tau^{-1} = AT + CT^{n} \quad (2)$$

where A, C, and n are coefficients and T is the temperature. The best fit was obtained with the parameters listed in Table 2. The results indicate that a dominant contribution from the Raman process involving both acoustic and optical phonons[9h] is responsible for the spin relaxation of complexes **1**−**3**.

Theoretical Studies. Compounds **1**−**3** were optimized using the XRD structure as an initial guess structure with the optimized geometries being in good agreement with the XRD structures (Tables S3−4). The same methodology was used to optimize other model complexes, which were used to predict anisotropy and magnetostructural studies. Initially, we performed anisotropy calculations on the XRD structures using the ORCA software suite to probe the effect of axial elongation and compression on the magnetic anisotropy of **1**−**3**. Although anisotropy calculations on six coordinate Co(II) complexes have been reported in the literature, small structural changes involving both axial and equatorial ligand(s) that serve to fine-tune both the sign and magnitude of D are still one of the open issues in the molecular magnetism community.[21] Although the sign of the NEVPT2/SA-CASSCF computed D for **1**−**3** is in agreement with the experimental findings, the magnitudes are larger than what was found experimentally (Table 3). It is well-known that the spin-conserved transition

Table 3. NEVPT2-Calculated (on the XRD Structures) D (cm^{-1}), E/D, g-Tensor, avg Co−X/Co−N Distance, and Energy Separation between KD1−KD2 and KD1−KD3 for Complexes 1−3[a]

	1	2	3
D (D_{KD1-2}, D_{KD1-3})	87.7 (47.1, 29.6)	127.0 (57.6, 36.4)	139.2 (52.7, 48.4)
E/D	0.19	0.15	0.02
g_{xx}, g_{yy}, g_{zz}	1.950, 2.420, 2.834	1.424, 1.961, 2.958	1.606, 2.218, 2.742
$\Delta E(1-2)$, $\Delta E(1-3)$	475, 897	68, 730	85, 473
Avg. (Co−X/Co−N) Distance Å (ea^{-1})	2.055/2.263	2.467/2.233	2.742/2.204

[a]The two values in the parentheses after D represent the contribution to D from the ground to first and ground to second exited state transitions, respectively.

between orbitals with the same m_l (magnetic quantum number) values contributes to a negative D value, whereas the transition between the orbitals of two different m_l values contributes to a positive D value.[10i] Large magnitudes of $|D|$ are to be expected when the energy difference between the orbitals involved in the transition is small and vice versa. For **1**−**3**, the dominant ground state electronic arrangement is found to be $(d_{yz})^2(d_{xz})^2(d_{xy})^1(d_{z^2})^1(d_{x^2-y^2})^1$ with 47%, 54% and 89% contributions, respectively. The ground state wave function for these compounds has a small contribution from other determinants (Figure S20).

The first and second exited states for **1**−**3**, which contribute the most to the D and E parameters, are also multideterminant in nature with $(d_{yz})^2(d_{xz})^1(d_{xy})^2(d_{z^2})^1(d_{x^2-y^2})^1$ and $(d_{yz})^2(d_{xz})^1(d_{xy})^1(d_{z^2})^1(d_{x^2-y^2})^2$ as the dominant electronic arrangements, respectively (Figure S20). Computed D values for **1**−**3** are estimated to be positive with the largest two contributions arising from $d_{xz} \rightarrow d_{xy}$ and $d_{xz} \rightarrow d_{x^2-y^2}$ transitions from ground to first and ground to second exited states, respectively (Figure 5). These findings are not

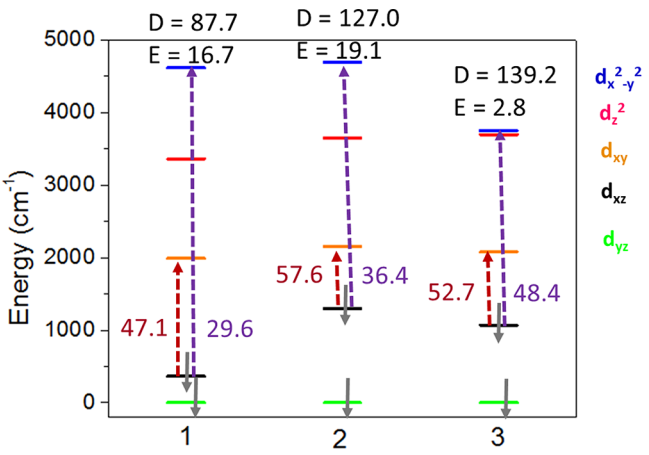

Figure 5. NEVPT2 computed d-orbital splittings for complexes **1**−**3**. The values written above the diagrams are computed D and E/D. Gray arrows represent beta electrons. Brick red and indigo color arrows represent dominant electronic transitions from ground to first ($d_{xz} \rightarrow d_{xy}$) and ground to second exited states, respectively ($d_{xz} \rightarrow d_{x^2-y^2}$).

unexpected, as the transitions occur between different m_l levels. Complexes **2** and **3** have almost double the magnitude of D compared to complex **1**. The value for **3** has a slightly higher magnitude compared to **2** (Figure 5 and Table 3) which can be rationalized on the basis of the energy separations between the d_{xz} and d_{xy} orbitals (1626, 854, and 1010 cm^{-1} for **1**−**3**, respectively, Figure 5) and between d_{xz} and $d_{x^2-y^2}$ orbitals (4253, 3395, and 2629 cm^{-1} for complexes **1**−**3**, respectively, Figure 5).

The larger the separation between the orbitals involved in the transition, the smaller the contribution will be to the magnitude of D and vice versa. For complexes **1**−**3**, the contribution to D from the $d_{xz} \rightarrow d_{xy}$ transition was found to be 47.1, 57.6, and 52.7 cm^{-1}, respectively (Figure 5, Table 3, and Tables S5−7). Whereas for the other dominant transition, between $d_{xz} \rightarrow d_{x^2-y^2}$, the contribution to the D parameter was found to be 29.6, 36.4, and 48.4 cm^{-1} for complexes **1**−**3**, respectively (Figure 5, Table 3, and Tables S5−7). The ground to first exited states and ground to second exited states contribution to the D parameter can also be correlated to the energy separation between these energy states ($\Delta E(1-2)$/$\Delta E(1-3)$, Table 3, Tables S5−7, and Figure S21). It is important to mention at this point that the SA-CASSCF and NEVPT2 computed D values have the same sign and trend for complexes **1**−**3**. Contributions to the D and E parameters due to spin-flip transitions are smaller for complexes **1**−**3** because of the larger energy separation between the quartet and doublet states (Figure S21 and Tables S5−7). The orientations of the D-matrices for complexes **1**−**3** are shown in Figure S22.

Anisotropy calculations on the H-optimized and fully optimized structures were also performed. For H-optimized structures, as expected, the anisotropy parameters were found to be very close to the XRD structures for all complexes (Table S8). For the fully optimized structures the sign of the D parameter was reproduced for all complexes but the magnitude is overestimated (Table S9). This is not unexpected given that

https://dx.doi.org/10.1021/acs.inorgchem.0c00531
Inorg. Chem. 2020, 59, 7622−7630

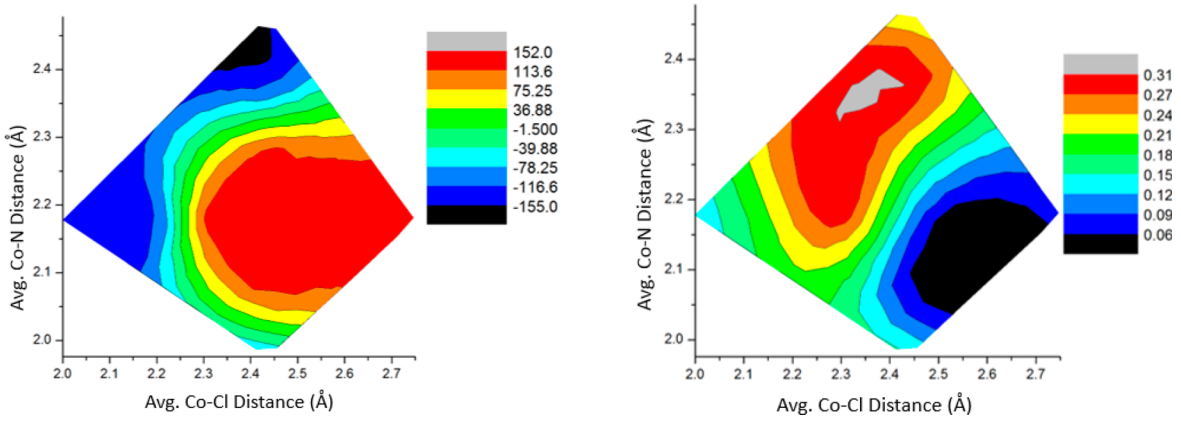

Figure 6. Magnetostructural correlation of D (left) and E/D (right) parameters performed on complex **2** by varying both axial and transverse ligand fields.

small structural deviations around the metal centers are known to alter the anisotropy parameters.[22]

To further understand the influence of both ligand fields on the magnetic anisotropy parameters, a magnetostructural correlation was performed on **2** with changes in the axial and transverse ligand fields while keeping other structural parameters the same. Magnetostructural studies suggest the possibility of attaining both axial and easy plane magnetic anisotropy by fine-tuning the ligand fields (Figure 6, Figure S23, and Table S10). An interesting finding is the prediction that certain ligand fields could lead to magnitudes of the $|D|$ parameter as high as $\sim \pm 150$ cm^{-1}. Indeed literature examples are known for Co(II) octahedral complexes with such large D values.[19b,23] In terms of the axial-to-equatorial bond length ratio (a/e or ae^{-1}), a small ratio of $\leq$1.02 is expected to lead to more negative D parameters and a ratio greater than 1.06 should lead to more positive D values (Figure S23). The other important parameter E/D, which represents the transverse component of the anisotropy, follows a parabolic trend with a maximum at ae^{-1} = 1.02 (Figure S23).

Given that the usage of the spin Hamiltonian may be ambiguous when SOC is too strong,[24] the HF-EPR analysis and calculations based on an S_{eff} = 1/2 effective spin model[25] were also performed to further corroborate the sign of magnetic anisotropy. As a result, the calculated g matrix was in reasonable agreement with those from HF-EPR (Table S11); both featured significantly smaller g_z compared to g_x or g_y. Therefore, the strong easy-plane character of the magnetic anisotropy is verified by both sets of spin Hamiltonian parameters.

CONCLUSIONS

Three six-coordinate mononuclear Co(II) complexes with distorted octahedral geometries were synthesized and fully characterized. In terms of the magnetostructural studies, the Co^{II} centers in all the complexes are located in a distorted octahedral geometry with similar equatorial pyridine coordination environments and axial ligands based on N, Cl, and Br atoms. The major difference is reflected in the axial distortion; namely, compression is observed for **1** and elongation for **2** and **3**. Magnetic, HF-EPR, and theoretical studies reveal easy-plane magnetic anisotropy for all the complexes with considerable spin−orbit coupling arising mainly from $d_{xz} \rightarrow d_{xy}$ and $d_{xz} \rightarrow d_{x^2-y^2}$ transitions and slow magnetic relaxation dominated by the Raman process involving both acoustic and optical phonons. These results support the conclusion that the easy-plane anisotropy of such cobalt(II) complexes with distorted octahedral geometries is maintained despite the modification of the axial ligands but that the magnitude of the zfs parameter is significantly changed. Moreover, magnetostructural studies performed on complex **2** hint at the possibility of attaining very large axial and easy plane magnetic anisotropy by fine-tuning the axial and equatorial ligand fields associated with the axial-to-equatorial bond length ratio. As such, the combined results of this study indicate that it is difficult to conclude that the D values vary regularly with the structural parameters such as the axial bond length or other donor properties because both the sign and magnitude of D are correlated with the electronic ground states.

ASSOCIATED CONTENT

Supporting Information

The Supporting Information is available free of charge at https://pubs.acs.org/doi/10.1021/acs.inorgchem.0c00531.

Experimental details, selected bond lengths and angles, crystal structures, magnetic measurements, HF-EPR data, and computational data (PDF)

Accession Codes

CCDC 1917525 contains the supplementary crystallographic data for this paper. These data can be obtained free of charge via www.ccdc.cam.ac.uk/data_request/cif, or by emailing data_request@ccdc.cam.ac.uk, or by contacting The Cambridge Crystallographic Data Centre, 12 Union Road, Cambridge CB2 1EZ, UK; fax: +44 1223 336033.

AUTHOR INFORMATION

Corresponding Authors

Yuan-Zhu Zhang − *Department of Chemistry, Southern University of Science and Technology, Shenzhen 518055, China;* orcid.org/0000-0002-1676-2427; Email: zhangyz@sustech.edu.cn

Kim R. Dunbar − *Department of Chemistry, Texas A & M University, College Station, Texas 77842, United States;* orcid.org/0000-0001-5728-7805; Email: dunbar@chem.tamu.edu

Authors

Yi-Fei Deng − *Department of Chemistry, Southern University of Science and Technology, Shenzhen 518055, China*

https://dx.doi.org/10.1021/acs.inorgchem.0c00531
Inorg. Chem. 2020, 59, 7622−7630

Mukesh Kumar Singh − *Department of Chemistry, Texas A & M University, College Station, Texas 77842, United States*
Dexuan Gan − *Department of Chemistry, Southern University of Science and Technology, Shenzhen 518055, China*
Tongtong Xiao − *Wuhan National High Magnetic Field Center & School of Physics, Huazhong University of Science and Technology, Wuhan 430074, P. R. China*
Yinuo Wang − *Department of Chemistry, Southern University of Science and Technology, Shenzhen 518055, China*
Shihao Liu − *Department of Chemistry, Southern University of Science and Technology, Shenzhen 518055, China*
Zhenxing Wang − *Wuhan National High Magnetic Field Center & School of Physics, Huazhong University of Science and Technology, Wuhan 430074, P. R. China;* orcid.org/0000-0003-2199-4684
Zhongwen Ouyang − *Wuhan National High Magnetic Field Center & School of Physics, Huazhong University of Science and Technology, Wuhan 430074, P. R. China*

Complete contact information is available at: https://pubs.acs.org/10.1021/acs.inorgchem.0c00531

Notes

The authors declare no competing financial interest.

■ ACKNOWLEDGMENTS

This work was supported by the National Natural Science Foundation of China (No. 21671095, 21901108, 21701046) and start-up fund from SUSTech. KRD and MKS gratefully acknowledge support for this work by the National Science Foundation (CHE-1808779) and the Welch Foundation (A-1449) for financial support. We also thank the HPRC at Texas A&M University for the computing resources and the Robert A. Welch Foundation (A-1449) and the Laboratory for Molecular Simulation and High-Performance Computing facilities at TAMU for providing software, support, and computer time.

■ REFERENCES

(1) (a) Gatteschi, D.; Sessoli, R.; Villain, J. *Molecular Nanomagnets*; Oxford University Press: 2006. (b) Sessoli, R.; Gatteschi, D.; Caneschi, A.; Novak, M. A. Magnetic Bistability in a Metal-Ion Cluster. *Nature* **1993**, *365*, 141−143.

(2) Mannini, M.; Pineider, F.; Sainctavit, P.; Danieli, C.; Otero, E.; Sciancalepore, C.; Talarico, A. M.; Arrio, M. A.; Cornia, A.; Gatteschi, D.; Sessoli, R. Magnetic memory of a single-molecule quantum magnet wired to a gold surface. *Nat. Mater.* **2009**, *8*, 194−197.

(3) (a) Leuenberger, M. N.; Loss, D. Quantum computing in molecular magnets. *Nature* **2001**, *410*, 789−793. (b) Hu, Z.; Dong, B.-W.; Liu, Z.; Liu, J.-J.; Su, J.; Yu, C.; Xiong, J.; Shi, D.-E.; Wang, Y.; Wang, B.-W.; Ardavan, A.; Shi, Z.; Jiang, S.-D.; Gao, S. Endohedral Metallofullerene as Molecular High Spin Qubit: Diverse Rabi Cycles in $Gd_2@C_{79}N$. *J. Am. Chem. Soc.* **2018**, *140*, 1123−1130. (c) Atzori, M.; Sessoli, R. The Second Quantum Revolution: Role and Challenges of Molecular Chemistry. *J. Am. Chem. Soc.* **2019**, *141*, 11339−11352.

(4) (a) Bogani, L.; Wernsdorfer, W. Molecular spintronics using single-molecule magnets. *Nat. Mater.* **2008**, *7*, 179−186. (b) Ganzhorn, M.; Klyatskaya, S.; Ruben, M.; Wernsdorfer, W. Strong spin−phonon coupling between a single-molecule magnet and a carbon nanotube nanoelectromechanical system. *Nat. Nanotechnol.* **2013**, *8*, 165−169.

(5) (a) Ishikawa, N.; Sugita, M.; Ishikawa, T.; Koshihara, S. y.; Kaizu, Y. Lanthanide Double-Decker Complexes Functioning as Magnets at the Single-Molecular Level. *J. Am. Chem. Soc.* **2003**, *125*, 8694−8695. (b) Woodruff, D. N.; Winpenny, R. E.; Layfield, R. A. Lanthanide single-molecule magnets. *Chem. Rev.* **2013**, *113*, 5110−5148. (c) Liddle, S. T.; van Slageren, J. Improving f-element single molecule magnets. *Chem. Soc. Rev.* **2015**, *44*, 6655−6669. (d) Liu, J.-L.; Chen, Y.-C.; Tong, M.-L. Symmetry strategies for high performance lanthanide-based single-molecule magnets. *Chem. Soc. Rev.* **2018**, *47*, 2431−2453. (e) Frost, J. M.; Harriman, K. L. M.; Murugesu, M. The rise of 3-d single-ion magnets in molecular magnetism: towards materials from molecules? *Chem. Sci.* **2016**, *7*, 2470−2491. (f) Feng, M.; Tong, M.-L. Single Ion Magnets from 3d to 5f: Developments and Strategies. *Chem. - Eur. J.* **2018**, *24*, 7574−7594.

(6) (a) Sessoli, R.; Tsai, H. L.; Schake, A. R.; Wang, J. B.; Folting, K.; Gatteschi, D.; Christou, G.; Hendrickson, D. N. High-spin molecules: $[Mn_{12}O_{12}(O_2CR)_{16}(H_2O)_4]$. *J. Am. Chem. Soc.* **1993**, *115*, 1804−1816. (b) Ako, A. M.; Hewitt, I. J.; Mereacre, V.; Clerac, R.; Wernsdorfer, W.; Anson, C. E.; Powell, A. K. A ferromagnetically coupled Mn_{19} aggregate with a record S = 83/2 ground spin state. *Angew. Chem., Int. Ed.* **2006**, *45*, 4926−4929. (c) Milios, C. J.; Vinslava, A.; Wernsdorfer, W.; Moggach, S.; Parsons, S.; Perlepes, S. P.; Christou, G.; Brechin, E. K. A record anisotropy barrier for a single-molecule magnet. *J. Am. Chem. Soc.* **2007**, *129*, 2754−2755.

(7) (a) Waldmann, O. A criterion for the anisotropy barrier in single-molecule magnets. *Inorg. Chem.* **2007**, *46*, 10035−10037. (b) Neese, F.; Pantazis, D. A. What is not required to make a single molecule magnet. *Faraday Discuss.* **2011**, *148*, 229−238.

(8) (a) Figgis, B. N.; Hitchman, M. A. *Ligand field theory and its applications*; Wiley-VCH: New York, 1999. (b) Chibotaru, L. F. Theoretical Understanding of Anisotropy in Molecular Nanomagnets. In *Molecular Nanomagnets and Related Phenomena*; Gao, S., Ed.; Springer Berlin Heidelberg: Berlin, Heidelberg, 2015; pp 185−229.

(9) (a) Jiang, S.-D.; Wang, B.-W.; Su, G.; Wang, Z.-M.; Gao, S.; Mononuclear Dysprosium, A. Complex Featuring Single-Molecule-Magnet Behavior. *Angew. Chem., Int. Ed.* **2010**, *49*, 7448−7451. (b) Jiang, S. D.; Wang, B. W.; Sun, H. L.; Wang, Z. M.; Gao, S. An Organometallic Single-Ion Magnet. *J. Am. Chem. Soc.* **2011**, *133*, 4730−4733. (c) Rinehart, J. D.; Long, J. R. Exploiting single-ion anisotropy in the design of f-element single-molecule magnets. *Chem. Sci.* **2011**, *2*, 2078−2085. (d) Zhang, P.; Zhang, L.; Wang, C.; Xue, S.; Lin, S.-Y.; Tang, J. Equatorially Coordinated Lanthanide Single Ion Magnets. *J. Am. Chem. Soc.* **2014**, *136*, 4484−4487. (e) Liu, J.; Chen, Y. C.; Liu, J. L.; Vieru, V.; Ungur, L.; Jia, J. H.; Chibotaru, L. F.; Lan, Y.; Wernsdorfer, W.; Gao, S.; Chen, X. M.; Tong, M. L. A Stable Pentagonal Bipyramidal Dy(III) Single-Ion Magnet with a Record Magnetization Reversal Barrier over 1000 K. *J. Am. Chem. Soc.* **2016**, *138*, 5441−50. (f) Chen, Y.-C.; Liu, J.-L.; Ungur, L.; Liu, J.; Li, Q.-W.; Wang, L.-F.; Ni, Z.-P.; Chibotaru, L. F.; Chen, X.-M.; Tong, M.-L. Symmetry-Supported Magnetic Blocking at 20 K in Pentagonal Bipyramidal Dy(III) Single-Ion Magnets. *J. Am. Chem. Soc.* **2016**, *138*, 2829−2837. (g) Ding, Y.-S.; Chilton, N. F.; Winpenny, R. E. P.; Zheng, Y.-Z. On Approaching the Limit of Molecular Magnetic Anisotropy: A Near-Perfect Pentagonal Bipyramidal Dysprosium(III) Single-Molecule Magnet. *Angew. Chem., Int. Ed.* **2016**, *55*, 16071−16074. (h) Goodwin, C. A. P.; Ortu, F.; Reta, D.; Chilton, N. F.; Mills, D. P. Molecular magnetic hysteresis at 60 K in dysprosocenium. *Nature* **2017**, *548*, 439−442. (i) Meng, Y.-S.; Xu, L.; Xiong, J.; Yuan, Q.; Liu, T.; Wang, B.-W.; Gao, S. Low-Coordinate Single-Ion Magnets by Intercalation of Lanthanides into a Phenol Matrix. *Angew. Chem., Int. Ed.* **2018**, *57*, 4673−4676. (j) Guo, F. S.; Day, B. M.; Chen, Y. C.; Tong, M. L.; Mansikkamaki, A.; Layfield, R. A. Magnetic hysteresis up to 80 K in a dysprosium metallocene single-molecule magnet. *Science* **2018**, *362*, 1400−1403. (k) Canaj, A. B.; Singh, M. K.; Regincós Marti, E.; Damjanović, M.; Wilson, C.; Céspedes, O.; Wernsdorfer, W.; Rajaraman, G.; Murrie, M. Boosting axiality in stable high-coordinate Dy(iii) single-molecule magnets. *Chem. Commun.* **2019**, *55*, 5950. (l) Canaj, A. B.; Dey, S.; Martí, E. R.; Wilson, C.; Rajaraman, G.; Murrie, M. Insight into D6h Symmetry: Targeting Strong Axiality in Stable Dysprosium(III) Hexagonal Bipyramidal Single-Ion Magnets. *Angew. Chem., Int. Ed.* **2019**, *58*, 14146−14151. (m) Canaj, A. B.; Singh, M. K.; Wilson, C.; Rajaraman,

G.; Murrie, M. Chemical and in silico tuning of the magnetisation reversal barrier in pentagonal bipyramidal Dy(iii) single-ion magnets. *Chem. Commun.* **2018**, *54*, 8273−8276. (n) Bar, A. K.; Kalita, P.; Singh, M. K.; Rajaraman, G.; Chandrasekhar, V. Low-coordinate mononuclear lanthanide complexes as molecular nanomagnets. *Coord. Chem. Rev.* **2018**, *367*, 163−216. (o) Singh, M. K.; Rajaraman, G. Acquiring a record barrier height for magnetization reversal in lanthanide encapsulated fullerene molecules using DFT and ab initio calculations. *Chem. Commun.* **2016**, *52*, 14047−14050. (p) Singh, M. K.; Yadav, N.; Rajaraman, G. Record high magnetic exchange and magnetization blockade in $Ln_2@C_{79}N$ (Ln = Gd(III) and Dy(III)) molecules: a theoretical perspective. *Chem. Commun.* **2015**, *51*, 17732−17735.

(10) (a) Freedman, D. E.; Harman, W. H.; Harris, T. D.; Long, G. J.; Chang, C. J.; Long, J. R. Slow Magnetic Relaxation in a High-Spin Iron(II) Complex. *J. Am. Chem. Soc.* **2010**, *132*, 1224−1225. (b) Zadrozny, J. M.; Long, J. R. Slow Magnetic Relaxation at Zero Field in the Tetrahedral Complex $[Co(SPh)_4]^{2-}$. *J. Am. Chem. Soc.* **2011**, *133*, 20732−20734. (c) Zadrozny, J. M.; Atanasov, M.; Bryan, A. M.; Lin, C.-Y.; Rekken, B. D.; Power, P. P.; Neese, F.; Long, J. R. Slow magnetization dynamics in a series of two-coordinate iron(ii) complexes. *Chem. Sci.* **2013**, *4*, 125−138. (d) Deng, Y.-F.; Han, T.; Wang, Z.; Ouyang, Z.; Yin, B.; Zheng, Z.; Krzystek, J.; Zheng, Y.-Z. Uniaxial magnetic anisotropy of square-planar chromium(ii) complexes revealed by magnetic and HF-EPR studies. *Chem. Commun.* **2015**, *51*, 17688−17691. (e) Meng, Y.-S.; Mo, Z.; Wang, B.-W.; Zhang, Y.-Q.; Deng, L.; Gao, S. Observation of the single-ion magnet behavior of d8 ions on two-coordinate Co(i)−NHC complexes. *Chem. Sci.* **2015**, *6*, 7156−7162. (f) Rechkemmer, Y.; Breitgoff, F. D.; van der Meer, M.; Atanasov, M.; Hakl, M.; Orlita, M.; Neugebauer, P.; Neese, F.; Sarkar, B.; van Slageren, J. A four-coordinate cobalt(II) single-ion magnet with coercivity and a very high energy barrier. *Nat. Commun.* **2016**, *7*, 10467. (g) Bar, A. K.; Pichon, C.; Sutter, J.-P. Magnetic anisotropy in two- to eight-coordinated transition−metal complexes: Recent developments in molecular magnetism. *Coord. Chem. Rev.* **2016**, *308*, 346−380. (h) Feng, X.; Hwang, S. J.; Liu, J.-L.; Chen, Y.-C.; Tong, M.-L.; Nocera, D. G. Slow Magnetic Relaxation in Intermediate Spin S = 3/2 Mononuclear Fe(III) Complexes. *J. Am. Chem. Soc.* **2017**, *139*, 16474−16477. (i) Singh, M. K.; Shukla, P.; Khatua, M.; Rajaraman, G. A Design Criteria to Achieve Giant Ising-Type Anisotropy in CoII-Encapsulated Metallofullerenes. *Chem. - Eur. J.* **2020**, *26*, 464−477.

(11) (a) Zadrozny, J. M.; Xiao, D. J.; Atanasov, M.; Long, G. J.; Grandjean, F.; Neese, F.; Long, J. R. Magnetic blocking in a linear iron (I) complex. *Nat. Chem.* **2013**, *5*, 577−581. (b) Yao, X. N.; Du, J. Z.; Zhang, Y. Q.; Leng, X. B.; Yang, M. W.; Jiang, S. D.; Wang, Z. X.; Ouyang, Z. W.; Deng, L.; Wang, B. W.; Gao, S. Two-Coordinate Co(II) Imido Complexes as Outstanding Single-Molecule Magnets. *J. Am. Chem. Soc.* **2017**, *139*, 373−380. (c) Bunting, P. C.; Atanasov, M.; Damgaard-Møller, E.; Perfetti, M.; Crassee, I.; Orlita, M.; Overgaard, J.; van Slageren, J.; Neese, F.; Long, J. R. A linear cobalt(II) complex with maximal orbital angular momentum from a non-Aufbau ground state. *Science* **2018**, *362*, eaat7319.

(12) (a) Gomez-Coca, S.; Cremades, E.; Aliaga-Alcalde, N.; Ruiz, E. Mononuclear single-molecule magnets: tailoring the magnetic anisotropy of first-row transition-metal complexes. *J. Am. Chem. Soc.* **2013**, *135*, 7010−7018. (b) Ruamps, R.; Batchelor, L. J.; Maurice, R.; Gogoi, N.; Jimenez-Lozano, P.; Guihery, N.; de Graaf, C.; Barra, A. L.; Sutter, J. P.; Mallah, T. Origin of the magnetic anisotropy in heptacoordinate Ni(II) and Co(II) complexes. *Chem. - Eur. J.* **2013**, *19*, 950−956.

(13) (a) Zhu, Y. Y.; Cui, C.; Zhang, Y. Q.; Jia, J. H.; Guo, X.; Gao, C.; Qian, K.; Jiang, S. D.; Wang, B. W.; Wang, Z. M.; Gao, S. Zero-field slow magnetic relaxation from single Co(II) ion: a transition metal single-molecule magnet with high anisotropy barrier. *Chem. Sci.* **2013**, *4*, 1802−1806. (b) Novikov, V. V.; Pavlov, A. A.; Nelyubina, Y. V.; Boulon, M. E.; Varzatskii, O. A.; Voloshin, Y. Z.; Winpenny, R. E. A Trigonal Prismatic Mononuclear Cobalt(II) Complex Showing Single-Molecule Magnet Behavior. *J. Am. Chem. Soc.* **2015**, *137*, 9792−9795. (c) Zhang, Y. Z.; Gomez-Coca, S.; Brown, A. J.; Saber, M. R.; Zhang, X.; Dunbar, K. R. Trigonal antiprismatic Co(ii) single molecule magnets with large uniaxial anisotropies: importance of Raman and tunneling mechanisms. *Chem. Sci.* **2016**, *7*, 6519−6527. (d) Palii, A. V.; Korchagin, D. V.; Yureva, E. A.; Akimov, A. V.; Misochko, E. Y.; Shilov, G. V.; Talantsev, A. D.; Morgunov, R. B.; Aldoshin, S. M.; Tsukerblat, B. S. Single-Ion Magnet Et_4N-$[Co^{II}(hfac)_3]$ with Nonuniaxial Anisotropy: Synthesis, Experimental Characterization, and Theoretical Modeling. *Inorg. Chem.* **2016**, *55*, 9696−9706. (e) Peng, Y.; Bodenstein, T.; Fink, K.; Mereacre, V.; Anson, C. E.; Powell, A. K. Magnetic anisotropy of a CoII single ion magnet with distorted trigonal prismatic coordination: theory and experiment. *Phys. Chem. Chem. Phys.* **2016**, *18*, 30135−30143. (f) Ozumerzifon, T. J.; Bhowmick, I.; Spaller, W. C.; Rappé, A. K.; Shores, M. P. Toward steric control of guest binding modality: a cationic Co(ii) complex exhibiting cation binding and zero-field relaxation. *Chem. Commun.* **2017**, *53*, 4211−4214. (g) Zhang, J.; Li, J.; Yang, L.; Yuan, C.; Zhang, Y.-Q.; Song, Y. Magnetic Anisotropy from Trigonal Prismatic to Trigonal Antiprismatic Co(II) Complexes: Experimental Observation and Theoretical Prediction. *Inorg. Chem.* **2018**, *57*, 3903−3912. (h) Yao, B.; Deng, Y.-F.; Li, T.; Xiong, J.; Wang, B.-W.; Zheng, Z.; Zhang, Y.-Z. Construction and Magnetic Study of a Trigonal-Prismatic Cobalt(II) Single-Ion Magnet. *Inorg. Chem.* **2018**, *57*, 14047−14051. (i) Hu, Z.-B.; Jing, Z.-Y.; Li, M.-M.; Yin, L.; Gao, Y.-D.; Yu, F.; Hu, T.-P.; Wang, Z.; Song, Y. Important Role of Intermolecular Interaction in Cobalt(II) Single-Ion Magnet from Single Slow Relaxation to Double Slow Relaxation. *Inorg. Chem.* **2018**, *57*, 10761−10767.

(14) (a) Craig, G. A.; Murrie, M. 3d single ion magnets. *Chem. Soc. Rev.* **2015**, *44*, 2135−2147. (b) Murrie, M. Cobalt(II) single-molecule magnets. *Chem. Soc. Rev.* **2010**, *39*, 1986−1995.

(15) Chilton, N. F.; Anderson, R. P.; Turner, L. D.; Soncini, A.; Murray, K. S. PHI: A powerful new program for the analysis of anisotropic monomeric and exchange-coupled polynuclear d- and f-block complexes. *J. Comput. Chem.* **2013**, *34*, 1164−1175.

(16) Krzystek, J.; Ozarowski, A.; Telser, J. Multi-frequency, high-field EPR as a powerful tool to accurately determine zero-field splitting in high-spin transition metal coordination complexes. *Coord. Chem. Rev.* **2006**, *250*, 2308−2324.

(17) Gatteschi, D.; Sessoli, R. Quantum tunneling of magnetization and related phenomena in molecular materials. *Angew. Chem., Int. Ed.* **2003**, *42*, 268−297.

(18) Guo, Y. N.; Xu, G. F.; Guo, Y.; Tang, J. Relaxation dynamics of dysprosium(III) single molecule magnets. *Dalton Trans.* **2011**, *40*, 9953−9963.

(19) (a) Zadrozny, J. M.; Liu, J.; Piro, N. A.; Chang, C. J.; Hill, S.; Long, J. R. Slow magnetic relaxation in a pseudotetrahedral cobalt(II) complex with easy-plane anisotropy. *Chem. Commun.* **2012**, *48*, 3927−3929. (b) Tesi, L.; Lunghi, A.; Atzori, M.; Lucaccini, E.; Sorace, L.; Totti, F.; Sessoli, R. Giant spin−phonon bottleneck effects in evaporable vanadyl-based molecules with long spin coherence. *Dalton. Trans.* **2016**, *45*, 16635−16643. (c) Lunghi, A.; Totti, F.; Sessoli, R.; Sanvito, S. The role of anharmonic phonons in under-barrier spin relaxation of single molecule magnets. *Nat. Commun.* **2017**, *8*, 14620. (d) Vallejo, J.; Castro, I.; Ruiz-Garcia, R.; Cano, J.; Julve, M.; Lloret, F.; De Munno, G.; Wernsdorfer, W.; Pardo, E. Field-induced slow magnetic relaxation in a six-coordinate mononuclear cobalt(II) complex with a positive anisotropy. *J. Am. Chem. Soc.* **2012**, *134*, 15704−15707. (e) Colacio, E.; Ruiz, J.; Ruiz, E.; Cremades, E.; Krzystek, J.; Carretta, S.; Cano, J.; Guidi, T.; Wernsdorfer, W.; Brechin, E. K. Slow magnetic relaxation in a Co(II)-Y(III) single-ion magnet with positive axial zero-field splitting. *Angew. Chem., Int. Ed.* **2013**, *52*, 9130−9134. (f) Gomez-Coca, S.; Urtizberea, A.; Cremades, E.; Alonso, P. J.; Camon, A.; Ruiz, E.; Luis, F. Origin of slow magnetic relaxation in Kramers ions with non-uniaxial anisotropy. *Nat. Commun.* **2014**, *5*, 4300.

(20) (a) Carlin, R. L.; Van Duyneveldt, A. J. *Magnetic Properties of Transition Metal Compounds*; Springer: New York, 1976. (b) Atzori, M.; Tesi, L.; Benci, S.; Lunghi, A.; Righini, R.; Taschin, A.; Torre, R.;

https://dx.doi.org/10.1021/acs.inorgchem.0c00531
Inorg. Chem. 2020, 59, 7622−7630

Sorace, L.; Sessoli, R. Spin Dynamics and Low Energy Vibrations: Insights from Vanadyl-Based Potential Molecular Qubits. *J. Am. Chem. Soc.* **2017**, *139*, 4338−4341.
(21) Titiš, J.; Boča, R. Magnetostructural D Correlations in Hexacoordinated Cobalt(II) Complexes. *Inorg. Chem.* **2011**, *50*, 11838−11845.
(22) Sarkar, A.; Tewary, S.; Sinkar, S.; Rajaraman, G. Magnetic Anisotropy in $Co^{II}X_4$ (X = O, S, Se) Single-Ion Magnets: Role of Structural Distortions versus Heavy Atom Effect. *Chem. - Asian J.* **2019**, *14*, 4696−4704.
(23) (a) Roy, S.; Oyarzabal, I.; Vallejo, J.; Cano, J.; Colacio, E.; Bauza, A.; Frontera, A.; Kirillov, A. M.; Drew, M. G.; Das, S. Two Polymorphic Forms of a Six-Coordinate Mononuclear Cobalt(II) Complex with Easy-Plane Anisotropy: Structural Features, Theoretical Calculations, and Field-Induced Slow Relaxation of the Magnetization. *Inorg. Chem.* **2016**, *55*, 8502−8513. (b) Varga, F.; Rajnak, C.; Titis, J.; Moncol, J.; Boca, R. Slow magnetic relaxation in a Co(ii) octahedral-tetrahedral system formed of a $[CoL_3]^{2+}$ core with L = bis(diphenylphosphanoxido) methane and tetrahedral $[CoBr_4]^{2-}$ counter anions. *Dalton. Trans.* **2017**, *46*, 4148−4151.
(24) Chibotaru, L. F. Theoretical Understanding of Anisotropy in Molecular Nanomagnets. *Struct. Bonding (Berlin, Ger.)* **2014**, *164*, 185−230.
(25) Chibotaru, L. F.; Ungur, L. Ab initio calculation of anisotropic magnetic properties of complexes. I. Unique definition of pseudospin Hamiltonians and their derivation. *J. Chem. Phys.* **2012**, *137*, 064112.

https://dx.doi.org/10.1021/acs.inorgchem.0c00531
Inorg. Chem. 2020, 59, 7622−7630